AAS 07-190

A permanent tethered observatory at Jupiter. Dynamical analysis

J. Peláez* and **D. J. Scheeres****

Abstract

Outer planet exploration has always been handicapped by a scarcity of power. The conversion from solar energy to electricity becomes rapidly ineffective further from the Sun. Solar intensity at Jupiter, the nearest of the outer planets, is only the 4% of its value at Earth. For a mission to Jupiter any extra power will allow the use of instruments which normally cannot be deployed in space because they need too much energy. Electrodynamic tethers could be used in some missions as an interesting alternative to produce the required level of onboard energy. This paper describes the essential dynamical issues arising in the placement of a permanent observatory located at one of the Jupiter inner moonlets (Adrastea, Metis, Amalthea) and sustained by an electrodynamic tether working in the generator regime. The electrodynamic tether will be *deorbiting* the moonlet by using its gravitational attraction; in doing so it converts the mechanical energy of the moonlet into electrical energy that can be used onboard. The aim of the work is to analyze the dynamical problem posed by such a observatory and also the main aspects related with the orbital dynamics and attitude dynamics of such a Jupiter station.

Introduction

Outer planet exploration has always been handicapped by a scarcity of power. The traditional means for powering long-duration space vehicles, solar energy converted to electricity, becomes rapidly ineffective as one travels further from the Sun. Solar intensity diminishes with the square of the distance from the Sun, so that at Jupiter, the nearest of the outer planets and five times more distant from the Sun than the Earth, the solar intensity is only one twenty-fifth its value at Earth. For a mission to Jupiter any extra power will allow the use of instruments which normally cannot be deployed in space because they need too much energy. This is one of the reasons why the JIMO mission of NASA investigated the use of nuclear-powered craft. Electrodynamic tethers could be used in some missions as an interesting alternative to produce the required level of onboard energy; particularly the bare tethers [1, 2]. This paper describes the essential dynamical issues arising in the placement of a permanent Jupiter observatory located at one of its inner moonlets (Adrastea, Metis, Amalthea) and sustained by an electrodynamic tether working in the generator regime.

When a system of mass m which is orbiting around a given planet descends from an initial orbit of radius a_i at $t = t_i$ to a final orbit of radius a_f at $t = t_f$ the mechanical energy lost in the process is given by

$$\Delta E = \frac{1}{2} m \mu \frac{a_i - a_f}{a_i a_f}$$

where μ is the gravitational constant of the planet. This is an approximate result obtained by assuming that the orbital system behaves as a point mass.

*Technical University of Madrid (UPM), School of Aeronautics, Madrid, E-28040, Spain.
E-mail address: j.pelaez@upm.es
**The University of Michigan, Aerospace Engineering, Ann Arbor, MI 48109, USA.
E-mail address: scheeres@umich.edu

The electrodynamic tethers can be used to deorbit satellites in different scenarios (see [3, 4, 5, 6]). If the descent has been carried out using an electrodynamic tether working in the generator regime this energy is dissipated through different mechanisms (see [7]). Roughly speaking, a part (E1) is spent bringing the electrons from the infinite to the tether. More energy (E2) is dissipated in the cathodic contactor of the tether. The ohmic losses in the conductive wire are another contribution (E3). Finally, a part (E4) is dissipated in any interposed load Z_T placed at the cathodic end of the tether.

This last contribution (E4) is, in fact, the useful energy, i.e., the energy that can be used onboard to perform some task (charging batteries, moving electrical engines or feeding some electronic circuit). Depending on the tether configuration, this contribution could reach 40% of the total energy (ΔE) lost in the deorbiting process; values around 20% would be considered quite reasonable. In this way, the electrodynamic tether becomes a source of electrical power which can be used to supply the whole system.

In fact, we are deorbiting the Jupiter moonlet, that is, its orbital radius will decrease; however, considering the huge mass of the inner moonlets it is possible to obtain large amounts of energy (ΔE) affecting the orbit of the moonlet in a negligible amount (small compared with 1 mm). Note that some link between the tether and the moonlet is required if we plan to deorbit the moonlet. In this case the gravity force due to the moonlet is playing the role of such a link. Adjusting the tether length, diameter and material it is possible to feed a permanent observatory of the Jupiter neighborhoods. The aim of the work is to analyze the dynamical problem posed by such a observatory and also the main aspects related with the orbital dynamics and attitude dynamics of such a Jupiter station.

Without a doubt, one of the greatest challenges facing such a mission is the extreme Jupiter radiation environment. This is a serious constraint that can be considered as a significant challenge for current or near-term developing technologies. Another problem is the uncertainty associated with the electronic plasma density in the neighborhoods of Jupiter; this is one of the important parameters in any mission using electrodynamic tethers, because the tether current strongly depends on this parameter. In the following we will not focus on these challenges, however.

Orbital dynamics

The analysis will start by describing the orbital dynamics of the S/C. In a first approximation there are three bodies involved in the problem: Jupiter, the inner moonlet and the S/C. Since all the moonlets have circular orbits around Jupiter (the eccentricity of the Amalthea orbit, for example, is $e \approx 0.003$), with very small inclination it is appropriate to consider the problem as a generalization of the classical circular restricted three body problem. To fix ideas we will assume that the moonlet is Amalthea; most of the analysis will be performed in non-dimensional variables and therefore the substitution for any other moonlet does not pose significant problems.

The form of Amalthea is extremely irregular with main dimensions of, approximately, $270 \times 165 \times 150$ km. Its gravitational field is also irregular. However, when more than 6 or 7 *diameters* from the satellite the gravitational field will be very close to the point mass potential. In what follows we will adopt this approximation for the gravitational field of the moonlet; later on, it would be possible to improve the analysis adopting more realistic values for it (for example, approximating the form of Amalthea by a triaxial ellipsoid or just using its lowest degree and order gravity field coefficients). In the particular case of Amalthea, it is stabilized by gravity gradient in its orbital frame with its longer axis along the local *vertical*. Its rotational and orbital periods coincide (both are equal to 0.498179 days).

The circular restricted three body problem

We summarize here the main results of the CRTBP involved in the analysis. Jupiter (m_1) and Amalthea (m_2) are the primaries and the S/C (m) has a negligible mass ($m << m_1$ and $m << m_2$). Any non rotating frame with origin at G, the center of mass of the primaries, is an inertial frame. The relative motion of primaries is circular and it takes place in a plane with constant direction.

Let Gx_1z_1 an inertial frame embedded in this plane. The synodic frame Gxz is rotating along the axis Gy with the angular velocity:

$$\omega = \sqrt{\frac{G(m_1 + m_2)}{\ell^3}}$$

where ℓ is the distance between both primaries (see Fig. 1); the primaries are at rest in the synodic frame $Gxyz$.

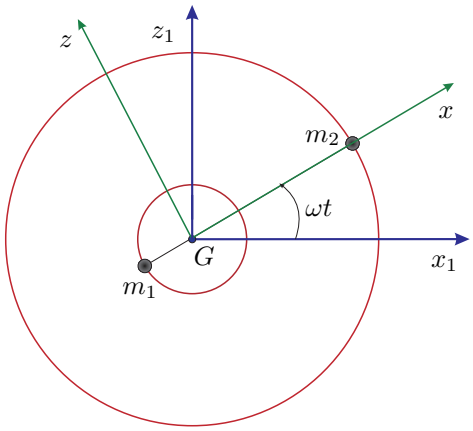

Figure 1: Circular restricted three body problem

Since we are interested in the motion of the S/C in the neighborhood of Amalthea (m_2) we will take a new frame $Axyz$ with origin at Amalthea and axis parallels to the corresponding axis of the frame $Gxyz$. Both frames correspond to the same rigid body. This new frame coincides with the orbital frame of Amalthea in its trajectory around Jupiter. Primaries are also at rest in this frame at positions $m_2(0,0,0), m_1(-\ell,0,0)$.

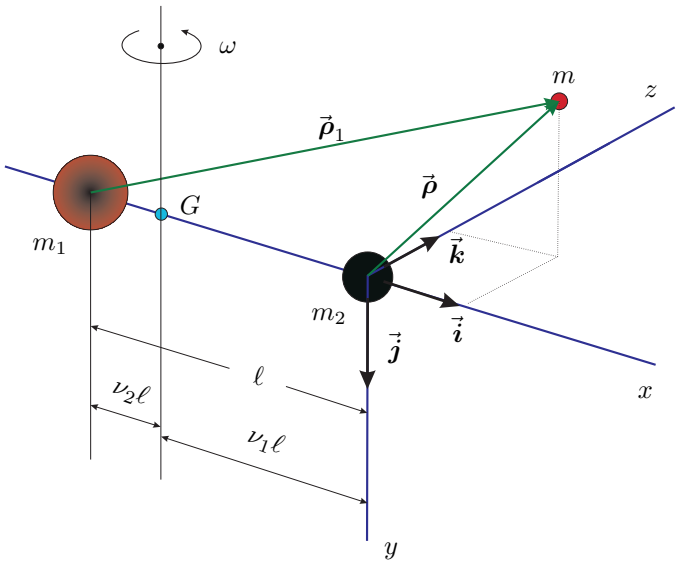

Figure 2: Reference frame

The motion of the S/C (m) relative to the frame $Axyz$ is governed by the following forces:

- *gravitational attraction of primaries*, given by

$$\vec{\boldsymbol{F}}_g = -\frac{Gm_1m}{\rho_1^3}\,\vec{\boldsymbol{\rho}}_1 - \frac{Gm_2m}{\rho^3}\,\vec{\boldsymbol{\rho}}$$

where $\vec{\boldsymbol{\rho}}_1 = (\ell + x, y, z)$, and $\vec{\boldsymbol{\rho}} = (x, y, z)$ are the position vectors of the mass m with origin at the primaries m_1 and m_2 respectively ($\rho = |\,\vec{\boldsymbol{\rho}}|$, $\rho_1 = |\,\vec{\boldsymbol{\rho}}_1|$). This force derive from the potential function

$$\tilde{V}_g = -Gm\{\frac{m_1}{\rho_1} + \frac{m_2}{\rho}\}$$

• *centrifugal force*, a repulsion of the Gy axis proportional to the mass and the distance; it derives from the potential function

$$\tilde{V}_I = -\frac{1}{2}m\omega^2((\ell + x)^2 + z^2)$$

• *inertial Coriolis force*, which is gyroscopic—it does not produce work in the motion of the S/C—and is given by

$$\vec{\boldsymbol{F}}_{1c} = -2m(-\omega\,\vec{\boldsymbol{j}}) \times \dot{\vec{\boldsymbol{\rho}}} = 2m\omega(\dot{z}, 0, -\dot{x})$$

• the *electrodynamic forces*, $\vec{\boldsymbol{f}}_e$, provided by the electrodynamic tether. Later on this will be modeled in detail.

Let $\tilde{V}$ be the resulting potential function $\tilde{V} = \tilde{V}_g + \tilde{V}_I$. The equations governing the motion of the particle m are:

$$m\ddot{x} - 2m\omega\dot{z} = -\frac{\partial\tilde{V}}{\partial x} + f_{ex} \tag{1}$$

$$m\ddot{z} + 2m\omega\dot{x} = -\frac{\partial\tilde{V}}{\partial z} + f_{ez} \tag{2}$$

$$m\ddot{y} = -\frac{\partial\tilde{V}}{\partial y} + f_{ey} \tag{3}$$

and they must be integrated from given initial conditions to yield the motion of the particle.

In the absence of electrodynamic forces, $\vec{\boldsymbol{f}}_e = \vec{\boldsymbol{0}}$, Eqns. (1-3) have the *Jacobi integral* which can be obtained from the energy equation. Indeed, the total energy of the system is constant

$$T + \tilde{V} = E \equiv \text{constante} \tag{4}$$

where $T = \frac{1}{2}mv^2$ is the kinetic energy of the particle in its motion relative to the frame $Axyz$.

Equations of motion

We will introduce non-dimensional variables taking into account the following characteristic values: for lengths, the distance ℓ between primaries, for time, $1/\omega$ ($\tau = \omega t$) and for masses, the total mass of the primaries $(m_1 + m_2)$. In *non dimensional* variables the equations of motion are:

$$\ddot{x} - 2\dot{z} = -\frac{\partial V}{\partial x} + kf_{ex} \tag{5}$$

$$\ddot{z} + 2\dot{x} = -\frac{\partial V}{\partial z} + kf_{ez} \tag{6}$$

$$\ddot{y} = -\frac{\partial V}{\partial y} + kf_{ey} \tag{7}$$

where $k = 1/(m\ell\omega^2)$, V is

$$V = -\frac{1}{2}((1 + x)^2 + z^2) - \frac{\nu}{\rho} - \frac{(1 - \nu)}{\rho_1} \tag{8}$$

and the reduced masses of primaries are $\nu = \nu_2 = m_2/(m_1 + m_2)$ and $(1 - \nu) = \nu_1 = m_1/(m_1 + m_2)$. Note that the positive direction of the Ax axis is from m_1 (Jupiter) to m_2 (Amalthea). Moreover, $\nu \ll 1$ since $m_2 \ll m_1$. From now on (x, y, z) stand for the non-dimensional coordinates of the S/C and the vectors $\vec{\boldsymbol{\rho}}_1$ and $\vec{\boldsymbol{\rho}}$ will be

$$\vec{\boldsymbol{\rho}}_1 = (1 + x, y, z) \qquad \vec{\boldsymbol{\rho}} = (x, y, z)$$

The Jacobi integral takes the form

$$\dot{x}^2 + \dot{y}^2 + \dot{z}^2 = h + (1 + x)^2 + z^2 + \frac{2\nu}{\rho} + \frac{2(1 - \nu)}{\rho_1} \tag{9}$$

In order to calculate the forces associated with the potential function V given by (8) the ratio $1/\rho_1$ should be determined. However,

$$\vec{\boldsymbol{\rho}}_1 = \vec{\boldsymbol{i}} + \vec{\boldsymbol{\rho}}$$

and therefore we have

$$\rho_1^2 = 1 + 2x + \rho^2, \qquad \frac{1}{\rho_1} = \frac{1}{\sqrt{1 + 2\,\vec{\boldsymbol{\rho}} \cdot \vec{\boldsymbol{i}} + \rho^2}}$$

Let ξ be one of the (x, y, z) coordinates of the vector $\vec{\boldsymbol{\rho}}$; the relations

$$\frac{\partial}{\partial \xi}(\rho) = \frac{\xi}{\rho}, \qquad \frac{\partial}{\partial \xi}(\frac{1}{\rho}) = -\frac{\xi}{\rho^3}$$

can be obtained directly. The derivatives involved in the equations take the values:

$$\frac{\partial \rho}{\partial x} = \frac{x}{\rho}, \qquad \frac{\partial \rho}{\partial y} = \frac{y}{\rho}, \qquad \frac{\partial \rho}{\partial z} = \frac{z}{\rho} \tag{10}$$

$$\frac{\partial}{\partial x}(\frac{1}{\rho}) = -\frac{x}{\rho^3}, \qquad \frac{\partial}{\partial y}(\frac{1}{\rho}) = -\frac{y}{\rho^3}, \qquad \frac{\partial}{\partial z}(\frac{1}{\rho}) = -\frac{z}{\rho^3} \tag{11}$$

$$\frac{\partial \rho_1}{\partial x} = \frac{1+x}{\rho_1}, \qquad \frac{\partial \rho_1}{\partial y} = \frac{y}{\rho_1}, \qquad \frac{\partial \rho_1}{\partial z} = \frac{z}{\rho_1} \tag{12}$$

$$\frac{\partial}{\partial x}(\frac{1}{\rho_1}) = -\frac{1+x}{\rho_1^3}, \qquad \frac{\partial}{\partial y}(\frac{1}{\rho_1}) = -\frac{y}{\rho_1^3}, \qquad \frac{\partial}{\partial z}(\frac{1}{\rho_1}) = -\frac{z}{\rho_1^3} \tag{13}$$

and the forces provided by the the potential function V are

$$-\frac{\partial V}{\partial x} = 1 + x - \nu\frac{x}{\rho^3} - (1-\nu)\frac{1+x}{\rho_1^3}$$
$$-\frac{\partial V}{\partial z} = z - \nu\frac{z}{\rho^3} - (1-\nu)\frac{z}{\rho_1^3}$$
$$-\frac{\partial V}{\partial y} = -\nu\frac{y}{\rho^3} - (1-\nu)\frac{y}{\rho_1^3}$$

The governing equations take the form

$$\ddot{x} - 2\dot{z} = 1 + x - \nu\frac{x}{\rho^3} - (1-\nu)\frac{1+x}{\rho_1^3} + kf_{ex} \tag{14}$$

$$\ddot{z} + 2\dot{x} = z - \nu\frac{z}{\rho^3} - (1-\nu)\frac{z}{\rho_1^3} + kf_{ez} \tag{15}$$

$$\ddot{y} \qquad = -\nu\frac{y}{\rho^3} - (1-\nu)\frac{y}{\rho_1^3} + kf_{ey} \tag{16}$$

and they are exact, within the limits of validity of the model.

Model for the electrodynamic forces

In a first approximation, we will assume the tether is stabilized by gravity gradient along the *local vertical of Jupiter*. Moreover, we will assume the tether is laying into the orbital plane of Amalthea (inclination 0.4°, practically zero). As a consequence the electrodynamic forces have a resultant contained into the orbital plane of Amalthea ($f_{ey} = 0$). In such a case, eq. (16) shows that the motion of the S/C takes place in the orbital plane Axz, ($y(t) \equiv 0$), if the initial conditions lay in the orbital plane ($y = \dot{y} = 0$). This is the situation that we are looking for.

Under these assumptions the resultant of the electrodynamic forces acting onto the S/C take the following nondimensional form

$$k\,\vec{\boldsymbol{f}}_e = \sigma\{-\sin\psi\,\vec{\boldsymbol{i}} + \cos\psi\,\vec{\boldsymbol{k}}\}, \quad \sigma = \frac{I_m B L}{m\ell\omega^2} \quad (17)$$

where the angle ψ is given by

$$\tan\psi = \frac{z}{1+x}, \quad \cos\psi = \frac{1+x}{\rho_1}, \quad \sin\psi = \frac{z}{\rho_1}$$

and $\rho_1 = \sqrt{(1+x)^2+z^2}$. In (17), L is the tether length, B the magnetic field in the center of mass of the S/C and I_m is the average tether current. The nondimensional parameter σ provides a measure of the magnitude of the electrodynamic forces. All parameters appearing in this subject can be obtained following the theories developed in [8, 9, 10, 11, 12].

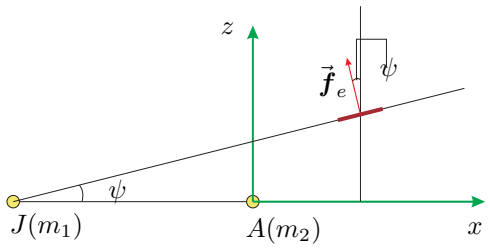

Figure 3: Resultant of the electrodynamic forces

Equilibrium position

We will determine the equilibrium position of the S/C in this scene. First of all, the value of ν is very small (for Amalthea $\nu \approx 3.79 \times 10^{-6}$) and the electrodynamic forces should be of the same order of magnitude. To begin with, we will neglect the electrodynamic forces and the gravitational attraction of the moonlet. Moreover, we will look for the equilibrium position which appear in the orbital plane of Amalthea.

Equilibrium without Amalthea and without tether

The equations governing the motion of the S/C into the orbital plane ($y = 0$) are:

$$\ddot{x} - 2\dot{z} = 1 + x - \frac{1+x}{\rho_1^3} \quad (18)$$

$$\ddot{z} + 2\dot{x} = z - \frac{z}{\rho_1^3} \quad (19)$$

The steady solutions of the eqs. (18-19) correspond to the equilibrium positions of the S/C relative to the frame $Axyz$. They are the roots of the system

$$(1+x)[1 - \frac{1}{\rho_1^3}] = 0, \qquad z[1 - \frac{1}{\rho_1^3}] = 0$$

which are given by the solution $\rho_1 = 1$, which corresponds to

$$\rho^2 + 2x = 0 \quad \Rightarrow \quad x^2 + z^2 + 2x = 0 \quad \Rightarrow \quad \boxed{(x+1)^2 + z^2 = 1}$$

As a consequence, the sought for equilibrium positions lay in the orbit of the moonlet. This result is quite reasonable: in the absence of electrodynamic forces and neglecting the gravitation of Amalthea, any satellite orbiting in the same trajectory than Amalthea will be in equilibrium relative to the frame $Axyz$.

Equilibrium with Amalthea and with an inert tether

Taking into account the gravitational forces from Amalthea, but assuming an inert tether, that is $\vec{\boldsymbol{f}}_e = \vec{\boldsymbol{0}}$, the equations (14-15) have five steady solutions: the five Lagrangian points $(L_1, L_2, \ldots, L_5)$ all of them situated into the orbital plane of Amalthea. The *triangular* solutions L_4 and L_5 are far

away from the moonlet (at distance ℓ) and they cannot be used in order to place there the tethered system.

The *rectilinear* solutions are roots of the equation

$$1 + x - \nu\frac{x}{\rho^3} - (1-\nu)\frac{1+x}{\rho_1^3} = 0$$

where $\rho = |x|$ and $\rho_1 = |1+x|$. Because of the very small value of ν these roots can be obtained by using asymptotic techniques. They are:

$$\begin{aligned}
L_1 \quad &\rightarrow \quad x_1 = +\frac{1}{3}(3)^{\frac{2}{3}}\nu^{\frac{1}{3}} + \frac{1}{9}(3)^{\frac{1}{3}}\nu^{\frac{2}{3}} - \frac{4}{27}\nu + \frac{14}{729}(3)^{\frac{2}{3}}\nu^{\frac{4}{3}} + \frac{70}{2187}(3)^{\frac{1}{3}}\nu^{\frac{5}{3}} + o(\nu^{\frac{5}{3}}) \\
L_2 \quad &\rightarrow \quad x_2 = -\frac{1}{3}(3)^{\frac{2}{3}}\nu^{\frac{1}{3}} + \frac{1}{9}(3)^{\frac{1}{3}}\nu^{\frac{2}{3}} - \frac{2}{27}\nu - \frac{22}{729}(3)^{\frac{2}{3}}\nu^{\frac{4}{3}} - \frac{16}{2187}(3)^{\frac{1}{3}}\nu^{\frac{5}{3}} + +o(\nu^{\frac{5}{3}}) \\
L_3 \quad &\rightarrow \quad x_3 = -2 + \frac{1}{4}\nu + \frac{1}{12}\nu^2 - \frac{103}{2304}\nu^3 + o(\nu^3)
\end{aligned}$$

The L_3 point is close to the opposite of Amalthea (relative to Jupiter) and it is not appropriate for our purpose. The other points, L_1 and L_2, are close to Amalthea. However, they are not appropriate because when the tether will be switched on the equilibrium would be broken due to transverse forces. To obtain a final answer we have to include the electrodynamic forces.

Equilibrium with Amalthea and with a live tether

When the gravitational forces of Amalthea and the electrodynamic forces are included in the analysis the equations providing the equilibrium positions are:

$$1 + x_e - \nu\frac{x_e}{\rho_e^3} - (1-\nu)\frac{1+x_e}{\rho_{1e}^3} - \sigma_0\frac{z_e}{\rho_{1e}} = 0 \tag{20}$$

$$z_e - \nu\frac{z_e}{\rho_e^3} - (1-\nu)\frac{z_e}{\rho_{1e}^3} + \sigma_0\frac{1+x_e}{\rho_{1e}} = 0 \tag{21}$$

where the electrodynamic forces have been modeled following the theory summarized previously. In these equations we will assume $\sigma_0 = \mathcal{O}(1)$. There are two free parameters in the problem, ν and σ_0, and there are two unknowns, x_e and z_e. Therefore, the roots of eqs. (20-21) that we are looking for take the form

$$x_e = x_e(\nu, \sigma_0), \qquad z_e = z_e(\nu, \sigma_0) \tag{22}$$

However, for a given moonlet, for example Amalthea, the value of ν is fixed and as a consequence the solutions only depend on σ_0, which is a measure of the intensity of the electrodynamic forces. For varying values of σ_0, the relations (22) represent a curve of the plane (x_e, z_e); each point of this curve provides an equilibrium position of the S/C relative to the frame $Axyz$.

The linear combinations $(-z_e)\times(20) + (1+x_e)\times$ (21) and $(z_e)\times(21) + (1+x_e)\times$ (20) provide the values of x_e and z_e as functions of ρ_e and ρ_{1e}:

$$z_e = \frac{\sigma_0}{\nu}\rho_e^3\rho_{1e}, \qquad x_e = \rho_e^2\{\frac{\rho_e}{\rho_{1e}} - 1\} + \frac{\rho_e^3}{\nu}\{\frac{\rho_{1e}^3 - 1}{\rho_{1e}}\}$$

Moreover, if we consider $\sigma_0 = \mathcal{O}(1)$ and the gravitational attraction of Amalthea must be compensated with the electrodynamic forces the distance of the S/C from Amalthea must be of order $\sqrt{\nu}$. Therefore we introduce the following variable

$$\xi_e = x_e/\sqrt{\nu}, \quad \zeta_e = z_e/\sqrt{\nu}, \quad \tilde{\rho_e} = \rho_e/\sqrt{\nu}$$

to make easier the numerical calculation of the roots.

The above relations become

$$\zeta_e = \sigma_0\tilde{\rho_e}^3\rho_{1e}, \qquad \xi_e = \tilde{\rho_e}^3\{\frac{\rho_{1e}^3 - 1}{\rho_{1e}}\} + \sqrt{\nu}\tilde{\rho_e}^2\{\sqrt{\nu}\frac{\tilde{\rho_e}}{\rho_{1e}} - 1\} \tag{23}$$

where the following relations should be taken into account:

$$\tilde{\rho_e} = \sqrt{\xi_e^2 + \zeta_e^2}, \quad \rho_{1e}^2 = 1 + 2\sqrt{\nu}\xi_e + \nu\tilde{\rho_e}^2 \tag{24}$$

Introducing the value of ζ_e (given by the first of the relations (23)) and ξ_e (given by the second of the relations (24)) into the equation $\tilde{\rho_e}^2 - \xi_e^2 - \zeta_e^2 = 0$ a new relationship linking $\tilde{\rho}_e$ and ρ_{1e} can be obtained. This new relation is a biquadratic equation for ρ_{1e} from which we can obtain the value of this last variable; it results

$$\rho_{1e}^2 = 1 + \nu\tilde{\rho}_e^2(1 - 2\sigma_0^2\tilde{\rho}_e^4) \pm 2\tilde{\rho}_e\sqrt{\tilde{\rho}_e^{10}\nu^2\sigma_0^4 - \nu\sigma_0^2\tilde{\rho}_e^4(\nu\tilde{\rho}_e^2 + 1) + \nu} \tag{25}$$

and it allows to express the coordinates (ξ_e, ζ_e) as a function of only $\tilde{\rho}_e$ through the equations (23).

The numerical procedure to calculate the roots is to create the function

$$g(\tilde{\rho}_e) = \tilde{\rho}_e^2 - \xi_e^2(\tilde{\rho}_e) - \zeta_e^2(\tilde{\rho}_e)$$

and to search for its zeroes. The procedure will be carried out as follows

1. We fix the value of σ_0
2. We calculate the zeroes of $g(\tilde{\rho}_e)$
3. For each one of these zeroes we obtain the value of ρ_{1e} (via relation (25))
4. The values of $\tilde{\rho}_e$ and ρ_{1e} allow to determinate the sought for roots (ξ_e, ζ_e) (via equations (23))
5. We change the value of σ_0 and we repeat the procedure

Two branches have been obtained. Figure 4 shows such branches in the plane (ξ_e, ζ_e) plus one additional curve, the greyed one, which is an asymptotic approximation to one of the branches (see equations (40-42) ahead). The parameter of each one of these curves is σ_0. On the *left* branch there is only one root which varies continuously with σ_0 in the range $[0, \infty]$; for $\sigma_0 \to 0$ this branch enters in the Lagrangian point L_2 and for $\sigma_0 \to \infty$ the branch approaches Amalthea. In the right branch, however, there are two different sub-branches for which σ_0 belongs to the range $\approx [0, 0.0312865]$ (there are no solutions for $\sigma_0 > 0.0312865$). For the lower sub-branch, when $\sigma_0 \to 0$ the equilibrium position approaches the Lagrangian point L_1; when $\sigma_0 \to 0.0312865$ the equilibrium position approaches the joining point J whose coordinates are, approximately, $J(0.80, 5.56)$. The upper sub-branch, however, is described in the opposite sense; thus, when $\sigma_0 \to 0$ the equilibrium position escapes from Amalthea through the axis Az and when $\sigma_0 \to 0.0312865$ the equilibrium position approaches the joining point J but from the other side.

Stability analysis

The steady solutions found in the previous section are unstable. From a physical point of view is simple to understand this unstable behavior. In any one of these equilibrium position the attraction from Amalthea is balanced by the electrodynamic forces. Any variation of the electrodynamic forces breaks the equilibrium and the S/C fall down into Amalthea or escapes far away from it.

However, it is convenient to perform a classical linear stability analysis in order to estimate the strength of the instability. This way it would be easier to introduce a control scheme on the system by compensating the terms that produce the instability; such terms are small in the neighborhood of the equilibrium position.

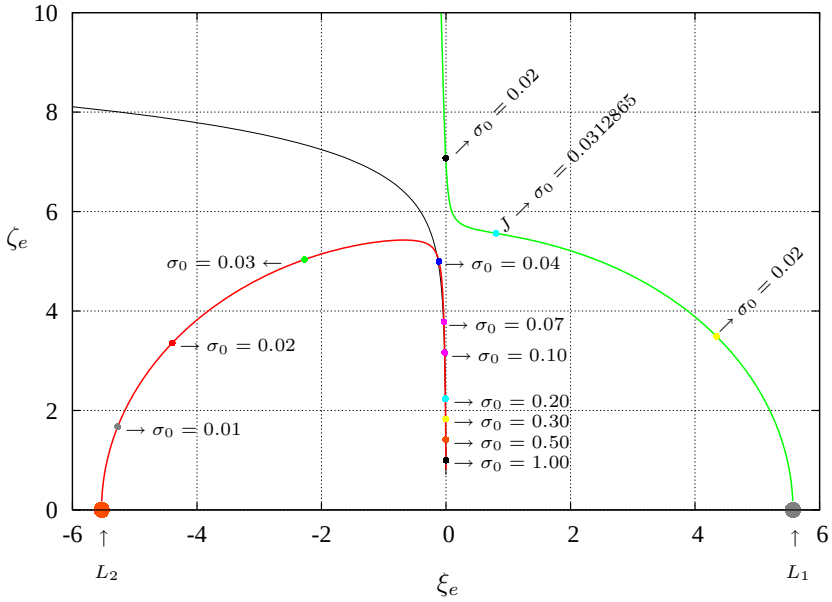

Figure 4: Equilibrium position in the plane (ξ_e, ζ_e)

Linear stability analysis

To study the linear stability of one equilibrium position we introduce the variations:

$$x(t) = x_e + \delta x, \qquad z(t) = z_e + \delta z$$

Since the orbital plane is an attractor we neglect, in a first approximation, the motion along the normal to the orbital plane (Ay axis). The variational equations of the system (14-15) adopt the form:

$$\frac{d^2\delta x}{d\tau^2} - 2\frac{d\delta z}{d\tau} + k_1\delta x + k_2\delta z = 0 \tag{26}$$

$$\frac{d^2\delta z}{d\tau^2} + 2\frac{d\delta x}{d\tau} + k_3\delta x + k_4\delta z = 0 \tag{27}$$

where the coefficients k_1, k_2, k_3 and k_4 are functions of the of the steady solution (x_e, z_e) obtained in the previous section; as a consequence, they are functions of (σ_0, ν) and take the following values:

$$k_1 = -1 - \frac{3\nu x_e^2}{\rho_e^5} + \frac{\nu}{\rho_e^3} - \frac{3(1-\nu)(1+x_e)^2}{\rho_{1e}^5} + \frac{(1-\nu)}{\rho_{1e}^3} - \sigma_0 z_e\frac{(1+x_e)}{\rho_{1e}^3} \tag{28}$$

$$k_2 = \frac{\sigma_0}{\rho_{1e}} - \frac{3\nu x_e z_e}{\rho_e^5} - \frac{\sigma_0 z_e^2}{\rho_{1e}^3} - \frac{3(1-\nu)(1+x_e)z_e}{\rho_{1e}^5} \tag{29}$$

$$k_3 = -\frac{3\nu x_e z_e}{\rho^5} - \frac{3(1-\nu)(1+x_e)z_e}{\rho_{1e}^5} + \frac{\sigma_0(1+x_e)^2}{\rho_{1e}^3} - \frac{\sigma_0}{\rho_{1e}} \tag{30}$$

$$k_4 = -1 - \frac{3(1-\nu)z_e^2}{\rho_{1e}^5} + \frac{\nu}{\rho^3} - \frac{3\nu z_e^2}{\rho^5} + \frac{(1-\nu)}{\rho_{1e}^3} + \frac{\sigma_0 z_e(1+x_e)}{\rho_{1e}^3} \tag{31}$$

The linear equation (26-27) can be rewritten in matrix form as follows

$$\frac{d\,\vec{\boldsymbol{y}}}{d\tau} = \mathcal{M}\,\vec{\boldsymbol{y}}$$

where $\mathcal{M}$ is the four-sized square matrix:

$$\mathcal{M} = \begin{pmatrix} 0, & 0, & 1, & 0 \\ 0, & 0, & 0, & 1 \\ -k_1, & -k_2, & 0, & 2 \\ -k_3, & -k_4, & -2, & 0 \end{pmatrix}$$

The secular equation of $\mathcal{M}$ is

$$\lambda^4 + (k_1 + k_4)\lambda^2 - 2(k_2 - k_3)\lambda + k_1 k_4 - k_2 k_3 = 0$$

and its roots provide the four eigenvalues of $\mathcal{M}$; they must be calculated numerically.

Eigenvalues of $\mathcal{M}$

Upper right sub-branch

The analysis will be started along the upper right sub-branch of the figure 4. When σ_0 takes increasing values (starting from zero) until the limiting value ≈ 0.0312865 we are *descending* by this sub-branch. Figure 5 shows the numerical values obtained for the eigenvalues of $\mathcal{M}$ as functions of σ_0.

For small values of σ_0 the eigenvalues are complex (two couples of conjugate complex number). This situation holds until σ_0 reaches the value ≈ 0.0311 beyond which all the eigenvalues take real values. Note that the eigenvalues $\lambda_{3,4}$ in figure 5 have a positive real part; as a consequence, the equilibrium position associated to this sub-branch are always unstable. However, the real part of this unstable eigenvalue is always in the range $\approx [0.6, 1.4]$.

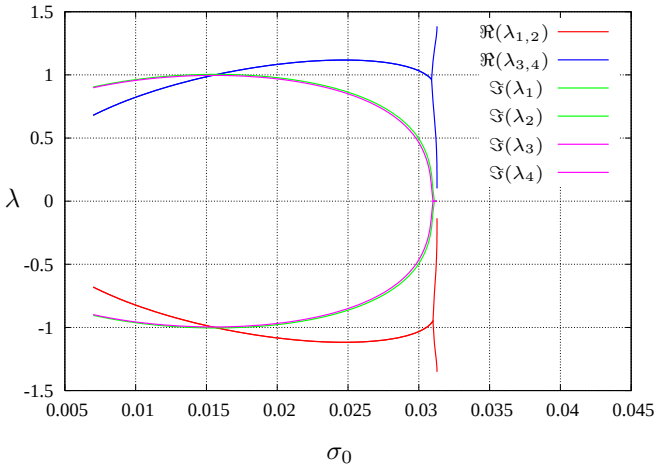

Figure 5: Real and imaginary parts of the eigenvalues of $\mathcal{M}$ vs. σ_0 (corresponding to the *upper right sub-branch*)

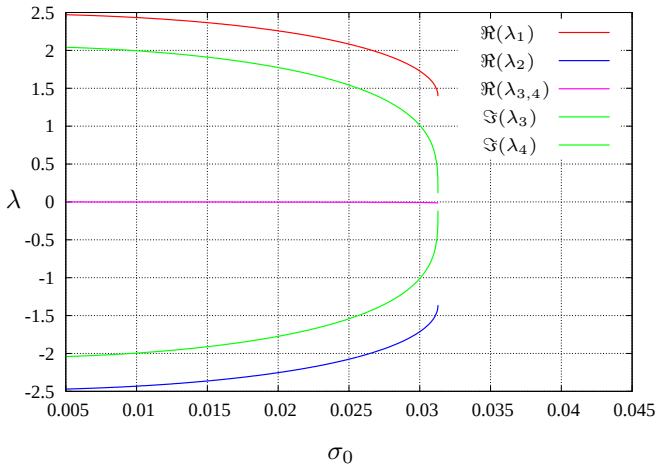

Figure 6: Real and imaginary parts of the eigenvalues of $\mathcal{M}$ vs. σ_0 (corresponding to the *lower right sub-branch*)

Lower right sub-branch

When σ_0 increases (starting from zero) until the limit value ≈ 0.0312865 we *ascend* by the lower right sub-branch of the figure 4. The numeric values obtained for the eigenvalues of the matrix $\mathcal{M}$ are summarized in figure 6 as functions of σ_0. For small values of σ_0 there are two real eigenvalues and one couple of conjugate complex numbers ($\lambda_{3,4}$); the real part of the complex eigenvalues is negative and very small (this detail cannot be realized in figure 6). One of the two real eigenvalues is always positive (λ_1) and it provides unstable character to these equilibrium positions. However, the unstable eigenvalue belong to the range $\approx [1.39, 2.5]$.

Left branch

Starting from $\sigma_0 = 0$ (L_2), and for increasing values of σ_0 we ascend by the left branch of the figure 4 when $\sigma_0 \in [0, 0.0332]$ (in approximation); then, when $\sigma_0 > 0.0332$ we descend by the branch

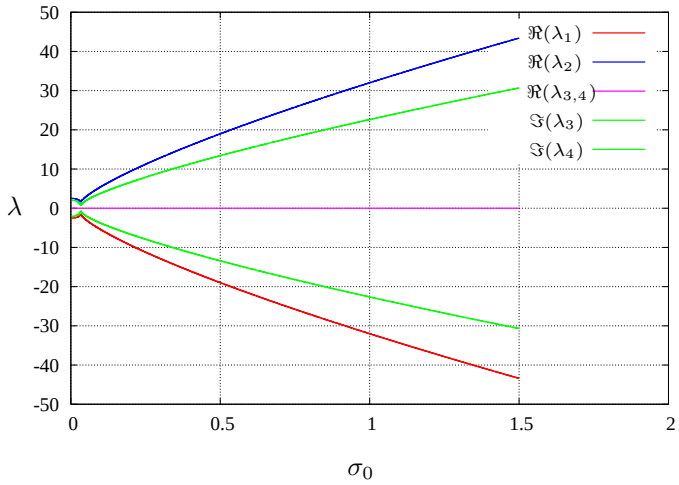

Figure 7: Real and imaginary parts of the eigenvalues of $\mathcal{M}$ vs. σ_0 (left branch)

approaching Amalthea. Figure 7 summarizes the numerical results obtained for the eigenvalues of $\mathcal{M}$ as functions of σ_0. There are two real eigenvalues and one complex conjugate pair ($\lambda_{3,4}$); the real part of the complex eigenvalues is negative and very small (this detail cannot be realized in figure 7). One of the real eigenvalues (λ_2) is always positive and it provides an unstable character to these equilibrium positions. In this branch the unstable eigenvalue reaches a minimum value ≈ 1.62287677 for $\sigma_0 \approx 0.033$; however, for increasing values of σ_0 the instability is much stronger than for the other branch: $\lambda_2 \in \approx [1.62, 44]$ when $\sigma_0 \in [0, 1.5]$. Therefore, this branch is more unstable than the right branch.

Asymptotic analysis

The governing equations (14-16) are *exact* within the limits of validity of our model. However, when the S/C is in the neighborhood of Amalthea, ρ, x, y and z take small values compared with unity. Therefore, we can deduce approximate equations governing the motion when it takes place in the vicinity of Amalthea continuously. For this, the terms associated with the centrifugal forces and the Jupiter attraction will be expanded in powers of the small parameter ρ. Let $\vec{\boldsymbol{f}}_d$ be the resultant of these forces; its components, in the frame $Axyz$ are:

$$
\begin{aligned}
f_{dx} &= 3x + \nu(1-2x) + \frac{3}{2}(1-\nu)(y^2+z^2-2x^2) + o(\rho^2) \\
f_{dy} &= -(1-\nu)y + 3(1-\nu)xz + o(\rho^2) \\
f_{dz} &= \nu z + 3(1-\nu)xz + o(\rho^2)
\end{aligned}
$$

Note that the electrodynamic forces (17) should be expanded also using the same level of approximation; therefore, the relations

$$\cos\psi \approx 1, \qquad \sin\psi \approx z$$

must be considered, providing a resultant

$$\vec{\boldsymbol{f}}_e \approx \sigma\{-z\,\vec{\boldsymbol{i}} + \vec{\boldsymbol{k}}\} \tag{32}$$

This way the following equations can be obtained

$$\ddot{x} - 2\dot{z} \approx -\nu\frac{x}{\rho^3} + 3x + \nu(1-2x) - \sigma z \tag{33}$$

$$\ddot{z} + 2\dot{x} \approx -\nu\frac{z}{\rho^3} + \nu z + \sigma \tag{34}$$

$$\ddot{y} \approx -\nu\frac{y}{\rho^3} - (1-\nu)y \tag{35}$$

where terms of order ρ^2 and smaller have been neglected.

Assuming σ_0 constant, the equilibrium position into the orbital plane are the roots of equations

$$-\nu\frac{x_e}{\rho_e^3} + 3x_e + \nu(1-2x_e) - \sigma_0 z_e = 0 \tag{36}$$

$$-\nu\frac{z_e}{\rho_e^3} + \nu z_e + \sigma_0 = 0 \tag{37}$$

We will introduce the following notation

$$\nu = \epsilon^2\sigma_0$$

where ϵ is small since $\sigma_0 = \mathcal{O}(1)$ and $\nu \ll 1$. The equation (37) provides z_e:

$$z_e = \frac{\rho_e^3}{\epsilon^2(1-\rho_e^3)} \tag{38}$$

From the equation (36-37) a linear combination can be obtained (eliminating the terms in $1/\rho_e^3$); it takes the form

$$\nu x_e z_e + \sigma_0 x_e - x_e z_e(3-2\nu) + \sigma_0 z_e^2 - \nu z_e = 0$$

and it provides the value of x_e, once the value of (38) is taken into account. This way we get:

$$x_e = \frac{\sigma_0\rho_e^3[\rho_e^3(1+\epsilon^4) - \epsilon^4]}{\epsilon^2(1-\rho_e^3)(\rho_e^3(3-2\sigma_0\epsilon^2) - \sigma_0\epsilon^2)} \tag{39}$$

Lastly, by introducing the values of (x_e, z_e) given by (38-39) into the identity:

$$(x_e^2 + z_e^2)^{\frac{3}{2}} - \rho_e^3 = 0$$

a relation $f(\rho_e, \epsilon, \sigma_0) = 0$ is obtained. Such a relation allows to determine $\rho_e = \rho_e(\epsilon, \sigma_0)$; "a posteriori", equations (38-39) provide the sought for values of (x_e, z_e).

This procedure can be combined with asymptotic techniques in the limit $\epsilon \to 0$. One solution obtained in this way takes the form:

$$\rho_e = \epsilon\{1 - \frac{1}{4}\epsilon^2 - \frac{3}{2\sigma_0}\epsilon^3 + \frac{3}{32}\frac{3\sigma_0^2 - 72 + 32\sigma_0}{\sigma_0^2}\epsilon^4 + o(\epsilon^5)\}$$

$$x_e = -\epsilon^2\{1 + \frac{3-\sigma_0}{\sigma_0}\epsilon - \frac{3}{2}\frac{\sigma_0^2 + 2\sigma_0 - 6}{\sigma_0^2}\epsilon^2 + \frac{1}{4}\frac{(63\sigma_0^2 + \sigma_0^3 + 36\sigma_0 - 108}{\sigma_0^3}\epsilon^3 + o(\epsilon^4)\}$$

$$z_e = \epsilon\{1 - \frac{3}{4}\epsilon^2 + (1 - \frac{9}{2\sigma_0})\epsilon^3 + \frac{3}{32}\frac{11\sigma_0^2 - 216 + 96\sigma_0}{\sigma_0^2}\epsilon^4 + o(\epsilon^5)\}$$

Note that in the plane (ξ_e, ζ_e), this solution coincides with a segment of the left branch described in figure 4 (specifically with the segment closet to the Az axis). Figure 4 shows the equilibrium position provided by this solution.

This solution provides the order of magnitude of the distance between the S/C and Amalthea in order to reach an equilibrium state with the tether working in the nominal regime (this nominal

regime should be determined). Rewriting the solution in terms of ν and neglecting terms of order ν^2 and smallers this solutions adopt the form

$$x_e = -\frac{\nu}{\sigma_0} + \frac{\sigma_0 - 3}{\sigma_0^{5/2}}\nu^{3/2} + \mathcal{O}(\nu^2) \tag{40}$$

$$z_e = \sqrt{\frac{\nu}{\sigma_0}} - \frac{3}{4}(\frac{\nu}{\sigma_0})^{3/2} + \mathcal{O}(\nu^2) \tag{41}$$

$$\rho_e = \sqrt{\frac{\nu}{\sigma_0}} - \frac{1}{4}(\frac{\nu}{\sigma_0})^{3/2} + \mathcal{O}(\nu^2) \tag{42}$$

The variational equations (26-27) can be used to study the linear stability analysis of this asymptotic solution. The coefficients $k_1, \ldots, k_4$ are functions of ν, σ_0, x_e and z_e given by the relations (28-31); their values can be obtained using the asymptotic solution (40-41). They take the form:

$$k_1 = \frac{\sigma_0^{3/2}}{\sqrt{\nu}} - 3 - \frac{13}{4}\sqrt{\sigma_0\nu} + \frac{16\sigma_0 - 27}{2\sigma_0}\nu + \mathcal{O}(\nu^{3/2}) \tag{43}$$

$$k_2 = 4\sigma_0 - \frac{3(\sigma_0 - 2)}{\sqrt{\sigma_0}}\sqrt{\nu} - \frac{(7\sigma_0^2 + 18\sigma_0 - 54)}{2\sigma_0^2}\nu + \mathcal{O}(\nu^{3/2}) \tag{44}$$

$$k_3 = 3\sigma_0 - \frac{3(\sigma_0 - 2)}{\sqrt{\sigma_0}}\sqrt{\nu} - \frac{(4\sigma_0^2 + 9\sigma_0 - 27)}{\sigma_0^2}\nu + \mathcal{O}(\nu^{3/2}) \tag{45}$$

$$k_4 = -\frac{2\sigma_0^{3/2}}{\sqrt{\nu}} + \frac{5}{2}\sqrt{\sigma_0\nu} - \frac{14\sigma_0 - 15}{2\sigma_0}\nu + \mathcal{O}(\nu^{3/2}) \tag{46}$$

It is very clear than the coefficients k_1 and k_4 are large compared with the other coefficients k_2 and k_3. By keeping only the more importante terms, the variational equations (26-27) take the following simplified form:

$$\frac{d^2\delta x}{d\tau^2} + \Omega^2\delta x = 0 \tag{47}$$

$$\frac{d^2\delta z}{d\tau^2} - 2\Omega^2\delta z = 0 \tag{48}$$

where Ω is given by

$$\Omega^2 = \frac{\sigma_0^{3/2}}{\sqrt{\nu}} \tag{49}$$

The eigenvalues of these equations are

$$\hat{\lambda}_1 = -\sqrt{2}\Omega, \quad \hat{\lambda}_2 = \sqrt{2}\Omega, \quad , \hat{\lambda}_{3,4} = \pm\Omega i$$

(here i is the imaginary unit). Now the behavior of some of the eigenvalues found in the previous section is clearer. By comparison with the numerical result (*exact*) summarized in figure 7: the real eigenvalues of that figure correspond to the eigenvalues $\hat{\lambda}_1$ and $\hat{\lambda}_2$ in this asymptotic analysis.

Figure 8 shows the eigenvalues of matrix $\mathcal{M}$ vs. σ_0 for the left branch described in figure 4; the results of both analysis (numerical and asymptotic) are plotted ($\lambda_1, \lambda_2, \lambda_{3,4}$ are numeric, $\hat{\lambda}_1, \hat{\lambda}_2, \hat{\lambda}_{3,4}$ are asymptotic). The agreement between both solutions is excellent, and it is almost impossible to detect the differences (even for small values of σ_0 where the differences are more remarkable).

Equations (47-48) have a simple solution:

$$\delta x(\tau) = A_1\cos(\Omega\tau + \phi_1), \qquad \delta z(\tau) = A_2\cosh(\sqrt{2}\Omega\tau + \phi_2)$$

The variation δx are periodic in a new time scale. The variation δz grows exponentially in the same time scale and depicts the unstable character of the equilibrium position around which we have

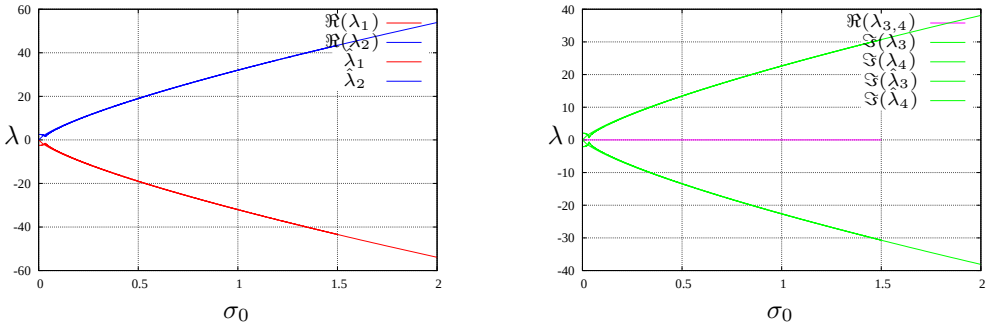

Figure 8: Real and imaginary parts of the eigenvalues of $\mathcal{M}$ vs. σ_0 (left branch) given by the numerical and the asymptotic analysis. Unstable eigenvalue (on the left)

linearized the system. It is important to note the new time scale which is associated with a new characteristics time $\tau_1 = \Omega\tau$. Since $\nu \ll 1$, $\Omega \gg 1$ and the characteristic times for which $\tau_1 = \mathcal{O}(1)$ correspond to very small time in the scale of τ. Therefore, the variation $(\delta x, \delta z)$ evolve in times clearly smaller than the orbital period of Amalthea around Jupiter. Lastly, the new time scale depends on the value of σ_0 and therefore on the nominal regime in which the tether should work.

Attitude dynamics

In that follows we will consider the angular momentum equation, relative to the center of mass of the tethered system, which governs its attitude dynamic. We assume that the tether is lying in the orbital plane of Amalthea and we will use the *dumbbell model* to simplify the mathematical analysis of the problem.

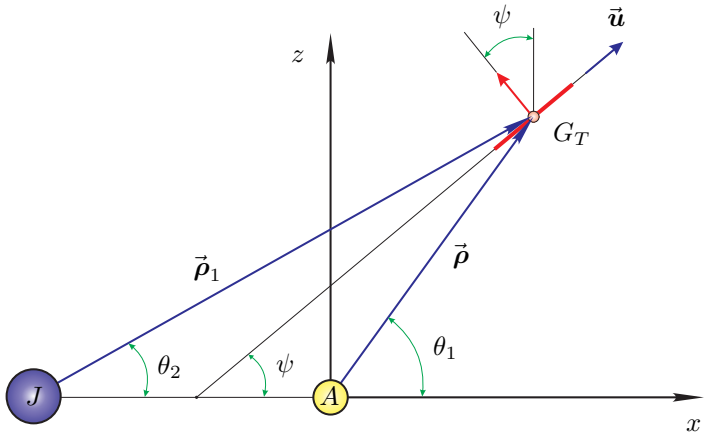

Figure 9: Tether attitude

Let G_T be the center of mass of the tethered system. Let $G_T x_1 y_1 z_1$ be a movable frame with origin at G_T and whose axes remain parallel to the corresponding axes of the inertial frame $G x_1 y_1 z_1$. By definition, the motion relative to the system center of mass G_T is the motion of the system relative to the frame $G_T x_1 y_1 z_1$, and it is governed by the angular momentum equation

$$\frac{d}{dt}(\vec{\boldsymbol{H}}_{G_T}) = \vec{\boldsymbol{M}}_{G_T} + \vec{\boldsymbol{M}}_E \tag{50}$$

where $\vec{\boldsymbol{H}}_{G_T}$ is the angular momentum of the tethered system given by $\vec{\boldsymbol{H}}_{G_T} = \bar{\bar{\mathbf{I}}}_{G_T} \circ \vec{\boldsymbol{\omega}}_T$. Here $\bar{\bar{\mathbf{I}}}_{G_T}$ is the central inertia tensor and $\vec{\boldsymbol{\omega}}_T$ is the angular velocity relative to the frame $G x_1 y_1 z_1$, and it takes the value[1]

$$\vec{\boldsymbol{\omega}}_T = \vec{\boldsymbol{u}} \times \dot{\vec{\boldsymbol{u}}} + \alpha\, \vec{\boldsymbol{u}} \tag{51}$$

where $\vec{\boldsymbol{u}}$ is a unit vector directed along the tether.

[1] In (51), the particular value of α is irrelevant because the moment of inertia relative to the tether line vanishes

On the right hand side of (50), we find the gravitational torque $\vec{M}_{G_T}$ produced by the primaries and the electrodynamic torque $\vec{M}_E$ produced by the electrodynamic forces. Both act in the system center of mass G_T. We will give expressions for these two torques shortly (equations (54-56)).

Since $\vec{u} \times \dot{\vec{u}}$ lies in a principal direction of inertia in G_T, the following relation holds

$$\bar{\bar{\mathbf{I}}}_{G_T} \circ \vec{\omega}_T = \bar{\bar{\mathbf{I}}}_{G_T} \circ (\vec{u} \times \dot{\vec{u}}) + \bar{\bar{\mathbf{I}}}_{G_T} \circ (\alpha \vec{u}) = I_s (\vec{u} \times \dot{\vec{u}})$$

where I_s is the moment of inertia of the tethered system about a line orthogonal to the tether through its center of mass G_T.

Thus, equation (50) takes the form

$$\vec{u} \times \ddot{\vec{u}} = \frac{1}{I_s}(\vec{M}_{G_T} + \vec{M}_E) \tag{52}$$

The derivative $\ddot{\vec{u}}$ must be calculated in the inertial frame, where the unit vectors $(\vec{i}_1, \vec{j}_1, \vec{k}_1)$ remain fixed. It takes the form

$$\ddot{\vec{u}} = \vec{u}'' + 2\vec{\omega} \times \vec{u}' + \vec{\omega} \times (\vec{\omega} \times \vec{u}) \tag{53}$$

where $\vec{u}'$ and $\vec{u}''$ are the time derivatives of $\vec{u}$ in the synodic frame and $\vec{\omega} = -\omega \vec{j}$ is the angular velocity of this synodic frame. Taking into account that

$$\vec{u} = (\cos\psi, 0, \sin\psi), \quad \vec{u}' = \dot{\psi}(-\sin\psi, 0, \cos\psi), \quad \vec{u}'' = \ddot{\psi}(-\sin\psi, 0, \cos\psi) + \dot{\psi}^2(-\cos\psi, 0, -\sin\psi)$$

and realizing that $\vec{\omega} \times \vec{u}' = \lambda \vec{u}$ and $\vec{\omega} \times (\vec{\omega} \times \vec{u}) = -\omega^2 \vec{u}$, it is possible to write

$$\vec{u} \times \ddot{\vec{u}} = \vec{u} \times \vec{u}'' = -\ddot{\psi} \vec{j}$$

The gravitational torque is given by

$$\vec{M}_{G_T} \approx \frac{3\mu_J}{\ell^3 \rho_1^5} \vec{\rho}_1 \times (\bar{\bar{\mathbf{I}}}_{G_T} \circ \vec{\rho}_1) + \frac{3\mu_A}{\ell^3 \rho^5} \vec{\rho} \times (\bar{\bar{\mathbf{I}}}_{G_T} \circ \vec{\rho})$$

where μ_J and μ_A are the gravitational constant of Jupiter and Amalthea, respectively. To obtain this expression, some assumptions have been made: 1) the gravitational field of primaries is perfectly spherical, and 2) when compared with unity, terms of order $L/\rho, L/\rho_1$—and higher—have been neglected.

The identity $\vec{a} = (\vec{a} \cdot \vec{u})\vec{u} + \vec{u} \times (\vec{a} \times \vec{u})$ leads to

$$\bar{\bar{\mathbf{I}}}_{G_T} \circ \vec{a} = I_s \vec{u} \times (\vec{a} \times \vec{u}) = I_s\{\vec{a} - \vec{u}(\vec{a} \cdot \vec{u})\}$$

and the gravitational torque turns out to be

$$\vec{M}_{G_T} \approx \frac{3\mu_J I_s}{\ell^3 \rho_1^5}(\vec{u} \times \vec{\rho}_1)(\vec{u} \cdot \vec{\rho}_1) + \frac{3\mu_A I_s}{\ell^3 \rho^5}(\vec{u} \times \vec{\rho})(\vec{u} \cdot \vec{\rho}) \tag{54}$$

In the right hand side of this expression appear the products:

$$\begin{aligned} \vec{u} \times \vec{\rho}_1 &= -\rho_1 \sin(\theta_2 - \psi)\vec{j}, & \vec{u} \cdot \vec{\rho}_1 &= \rho_1 \cos(\theta_2 - \psi) \\ \vec{u} \times \vec{\rho} &= -\rho \ \sin(\theta_1 - \psi)\vec{j}, & \vec{u} \cdot \vec{\rho} &= \rho \ \cos(\theta_1 - \psi) \end{aligned}$$

which permit to write the gravitational torque as

$$\vec{M}_{G_T} \approx -\left(\frac{3\mu_J I_s}{\ell^3}\frac{1}{\rho_1^3}\sin(2(\theta_2 - \psi)) + \frac{3\mu_A I_s}{\ell^3}\frac{1}{\rho^3}\sin(2(\theta_1 - \psi))\right)\vec{j}$$

Taking into account that

$$\frac{\mu_A}{\mu_J + \mu_A} = \nu, \qquad \frac{\mu_J}{\mu_J + \mu_A} = 1 - \nu$$

we obtain the final expression

$$\vec{\boldsymbol{M}}_{G_T} \approx -I_s\omega^2 \left(\frac{1-\nu}{\rho_1^3} \sin(2(\theta_2 - \psi)) + \frac{\nu}{\rho^3} \sin(2(\theta_1 - \psi)) \right) \vec{\boldsymbol{j}} \tag{55}$$

The torque about G_T introduced by the electrodynamic forces is

$$\vec{\boldsymbol{M}}_E = \vec{\boldsymbol{u}} \times (\vec{\boldsymbol{u}} \times \vec{\boldsymbol{B}}) J_1, \qquad \text{where} \quad J_1 = \int_0^L (h_G - h) I_e(h) dh \tag{56}$$

$I_e(h)$ is the tether current profile and $\vec{\boldsymbol{B}}$ is the Jupiter magnetic field, which will be considered constant along the tether (and equal to its value in G_T). The orbit of Amalthea is, practically, on the equatorial plane of Jupiter (inclination 0.4°); therefore, assuming an aligned dipole model for the Jupiter magnetic field we have:

$$\vec{\boldsymbol{B}} = b\,\vec{\boldsymbol{j}}, \quad \Rightarrow \quad \vec{\boldsymbol{M}}_E = -BJ_1\,\vec{\boldsymbol{j}}$$

The angular momentum equation takes the following non-dimensional form:

$$\ddot{\psi} = \frac{1-\nu}{\rho_1^3} \sin(2(\theta_2 - \psi)) + \frac{\nu}{\rho^3} \sin(2(\theta_1 - \psi)) + \frac{BJ_1}{I_s\omega^2} \tag{57}$$

Equation (57) should be integrated together with equations (14-15) since all of them are coupled; note that the values of the angles θ_1 and θ_2 depend on the coordinates (x, z) through the following relations

$$\sin\theta_1 = \frac{z}{\rho}, \qquad \sin\theta_2 = \frac{z}{\rho_1}$$
$$\cos\theta_1 = \frac{x}{\rho}, \qquad \cos\theta_2 = \frac{1+x}{\rho_1}$$

We will assume, in a first analysis that the tether is self-balanced, and as a consequence $\vec{\boldsymbol{M}}_E = \vec{\boldsymbol{0}}$; in such a case, it should be notice that in the limit $\nu \to 0$ the equilibrium position provides by equation (57) is

$$\sin(2(\theta_2 - \psi)) = 0 \quad \Rightarrow \quad \psi = \theta_2$$

This result justify the analysis performed in previous section which results as a first approximation to a more detailed solution.

Equilibrium positions

Considering the attitude dynamics the equilibrium positions are steady solutions of the system formed by Eqns. (14,15,57). As a consequence they are roots of the following problem:

$$0 = 1 + x_e - \nu\frac{x_e}{\rho_e^3} - (1-\nu)\frac{1+x_e}{\rho_{1e}^3} - \sigma\sin\psi_e \tag{58}$$

$$0 = z_e - \nu\frac{z_e}{\rho_e^3} - (1-\nu)\frac{z_e}{\rho_{1e}^3} + \sigma\cos\psi_e \tag{59}$$

$$0 = \frac{1-\nu}{\rho_{1e}^3} \sin(2(\theta_{2e} - \psi_e)) + \frac{\nu}{\rho_e^3} \sin(2(\theta_{1e} - \psi_e)) \tag{60}$$

They are functions of the non-dimensional parameters σ and ν

$$x_e = x_e(\sigma, \nu), \quad z_e = z_e(\sigma, \nu), \quad \psi_e = \psi_e(\sigma, \nu)$$

which must be obtained numerically.

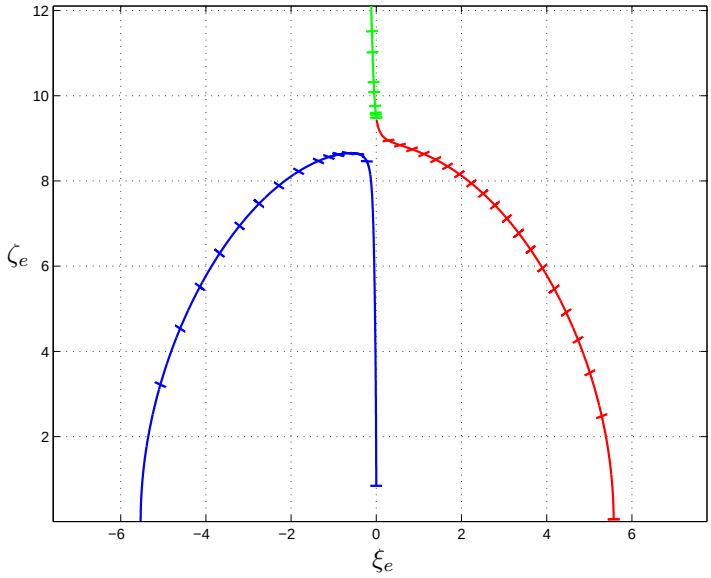

Figure 10: Equilibrium position and tether attitude

Figure 10 shows the equilibrium position in the plane ($\xi_e = x_e/\sqrt{\nu}, \zeta_e = z_e/\sqrt{\nu}$) and also the orientation of the tether, given by ψ_e in some particular cases. Note that from a qualitative point of view figure 10 is similar to figure 4, which shows the equilibrium positions when $\psi_e = \theta_{2e}$. However, there are differences that should be remarked.

In the left branch of the figure, and starting from the Lagrangian point L_2 where $\sigma_0 = 0$, the parameter σ_0 increases continuously until reach a relative maximum value: $\sigma_{0_{max}} \approx 0.02065$ at ($\xi_e \approx -4.06261, \zeta_e \approx 5.66127$); then, the value of σ_0 starts to decrease until reach a relative minimum value: $\sigma_{0_{min}} \approx 0.01345$ at ($\xi_e \approx -0.50272, \zeta_e \approx 8.64990$). Behind $\sigma_{0_{min}}$ the value of σ_0 increases unbounded until reach the origin (Amalthea) when $\sigma_0 \to \infty$.

On the right branch and starting from the Lagrangian point L_1 where $\sigma_0 = 0$, the parameter σ_0 increases continuously until reach a relative maximum value: $\sigma_{0_{max}} \approx 0.02022$ at ($\xi_e \approx 4.01445, \zeta_e \approx 5.76223$). Behind this maximum value, σ_0 decreases unbounded while the S/C separates more and more from Amalthea.

In both branches, and along the positions which are the closet to the Az axis, the tether remains *almost parallel* to the Ax axis.

Linear stability analysis

To study the linear stability of one equilibrium position we introduce the variations:

$$x(t) = x_e + \delta x, \qquad z(t) = z_e + \delta z, \qquad \psi(t) = \psi_e + \delta\psi$$

Since the orbital plane is an attractor we neglect, in a first approximation, the motion along the normal to the orbital plane (Ay axis). The variational equations of the system adopt the form:

$$\frac{d^2\delta x}{d\tau^2} - 2\frac{d\delta z}{d\tau} + k_{11}\delta x + k_{12}\delta z + k_{13}\delta\psi = 0 \tag{61}$$

$$\frac{d^2\delta z}{d\tau^2} + 2\frac{d\delta x}{d\tau} + k_{21}\delta x + k_{22}\delta z + k_{23}\delta\psi = 0 \tag{62}$$

$$\frac{d^2\delta\psi}{d\tau^2} + k_{31}\delta x + k_{32}\delta z + k_{33}\delta\psi = 0 \tag{63}$$

where the coefficients $k_{11}, \ldots, k_{33}$ are functions of the of the steady solution (x_e, z_e, ψ_e) obtained in the previous section; as a consequence, they are functions of (σ_0, ν). The linear equations (61-63) can

be rewritten in matrix form as follows

$$\frac{d\,\vec{\boldsymbol{y}}}{d\tau} = \mathcal{M}\,\vec{\boldsymbol{y}}$$

where $\mathcal{M}$ is the six-sized square matrix:

$$\mathcal{M}(\sigma_0,\nu) = \begin{pmatrix} 0, & 0, & 0, & 1, & 0, & 0 \\ 0, & 0, & 0, & 0, & 1, & 0 \\ 0, & 0, & 0, & 0, & 0, & 1 \\ -k_{11}, & -k_{12}, & -k_{13} & 0, & 2, & 0 \\ -k_{21}, & -k_{22}, & -k_{23}, & -2, & 0, & 0 \\ -k_{31}, & -k_{32}, & -k_{33}, & 0, & 0, & 0 \end{pmatrix}$$

The eigenvalues of matrix $\mathcal{M}$ provide the stability properties of the equilibrium positions. In general there are three pairs of conjugate complex numbers which are functions of (σ_0,ν); in some cases some eigenvalues could take real values. In any case these eigenvalues should be calculated numerically.

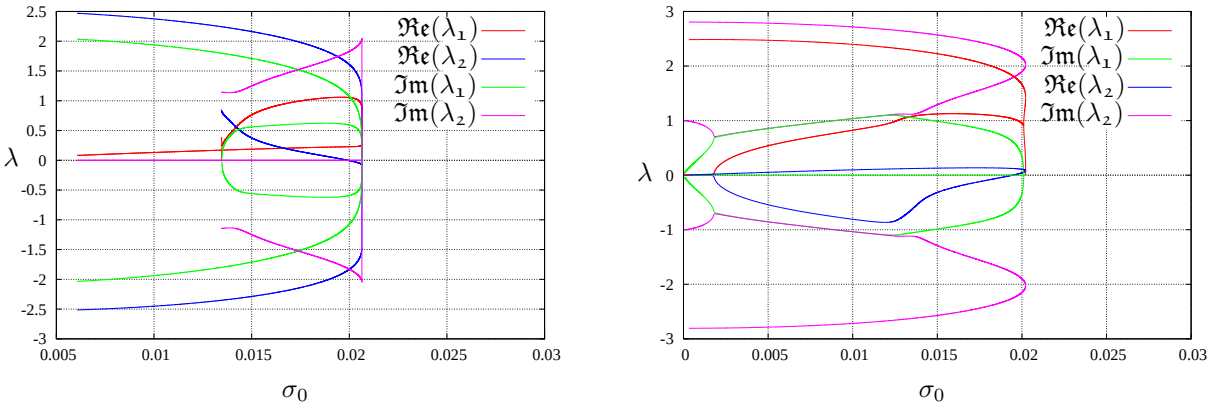

Figure 11: Eigenvalues *with positive real part* vs. σ_0 (Left branch on the left, right branch on the right)

Figure 11 shows the eigenvalues with positive real part as functions of σ_0 for the particular case of Amalthea ($\nu =\approx 3.792053878\times 10^{-6}$). The plot on the right side corresponds to the equilibrium positions in the right branch of figure 10. The real part of most unstable eigenvalue is in the range $\approx [1, 2.5]$; therefore, these equilibrium positions are unstable but there are more unstable equilibrium positions localized in the left branch. The plot on the left side corresponds to the equilibrium positions in one segment of the left branch of figure 10; specifically for the equilibrium positions which appear when σ_0 ranges in the interval $[0, \sigma_{0_{min}}]$ (this interval contains the relative maximum $\sigma_{0_{max}}$ inside). The real part of most unstable eigenvalue is in the range $\approx [1, 2.5]$, that is, strength of the instability is similar to the previous case.

The left plot in figure 12 also shows the eigenvalues with positive real part as functions of σ_0 but now, the plot corresponds to the equilibrium positions in a segment of the left branch of figure 10 which appears when $\sigma_0 \in [\sigma_{0_{min}}, \infty]$. For these equilibrium positions, the real part of the most unstable eigenvalue is one order of magnitude larger than in the previous cases shown in figure 11; therefore, they are the most unstable. However, they are also the most interesting because for them the tether remains practically parallel to the axis Ax as you can see in the same figure 12 (right plot) where the values of ψ_e versus σ_0 have been plotted for these equilibrium positions. This set of solutions will be called the *main set* to distinguish it from the remainder solutions.

Asymptotic analysis

It is possible to obtain an asymptotic solution for the equilibrium positions belonging to the main set. Indeed, an analysis similar to the one carried out in a previous section provides the following

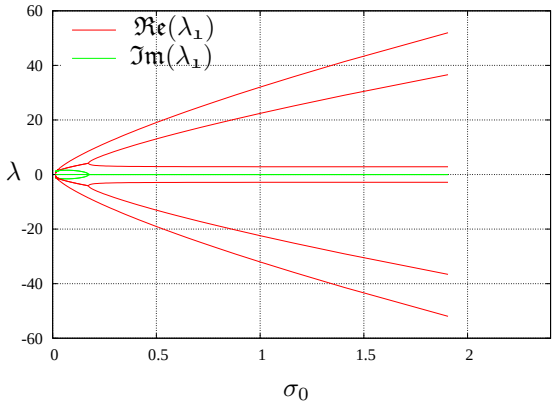

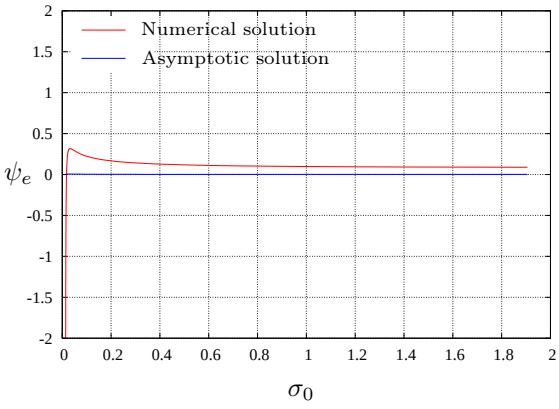

Figure 12: On the left: eigenvalues *with positive real part* vs. σ_0 (main set). On the right: tether attitude ψ_e, degrees, vs. σ_0 in the equilibrium (main set)

solution:

$$x_e = -\frac{5+2\sigma_0}{8}\cdot\frac{\nu}{\sigma_0} + \frac{2\sigma_0-3}{32\sigma_0}\cdot(\frac{\nu}{\sigma_0})^{3/2} + \mathcal{O}(\nu^2) \tag{64}$$

$$z_e = \sqrt{\frac{\nu}{\sigma_0}} - \frac{4\sigma_0^2+20\sigma_0+25}{128}\cdot(\frac{\nu}{\sigma_0})^{3/2} + \mathcal{O}(\nu^2) \tag{65}$$

$$\psi_e = \frac{5+2\sigma_0}{8}\sqrt{\frac{\nu}{\sigma_0}} + \frac{6\sigma_0-9}{32\,\sigma_0}\cdot\frac{\nu}{\sigma_0} + \frac{8\sigma_0^5+228\sigma_0^4+30\sigma_0^3+215\sigma_0^2+432\sigma_0-648}{3072\,\sigma_0^2}\cdot(\frac{\nu}{\sigma_0})^{3/2} + \mathcal{O}(\nu^2) \tag{66}$$

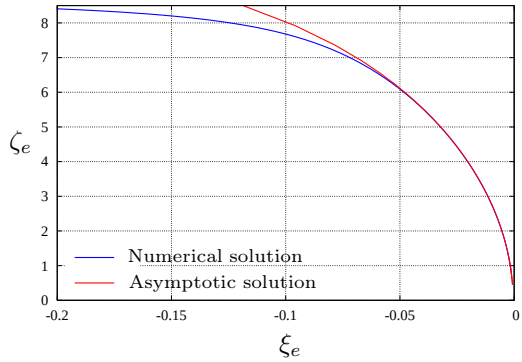

Figure 13: The main set

The agreement between this solution and the numerical solution is very good, as you can see in the figure 13. This asymptotic solution allows a more detailed study of the linear stability properties of this space system. In effect, the coefficients $k_{11},\ldots,k_{33}$ which appears in equations (61-63) can be calculated analytically in terms of the free parameters of the problem (σ_0,ν). The are given in Table 1 (see page 1326). In the limit $\nu\to 0$ the more important terms are

$$k_{11}=\Omega^2,\quad k_{22}=-2\Omega^2,\quad k_{31}=-\frac{2}{\sigma_0}\Omega^4$$
$$k_{32}=-\frac{5+2\sigma_0}{4}\Omega^2,\quad k_{33}=-2\Omega^2$$

where Ω is given by (49). Therefore, the variational equations (61-63) take the following simplified form

$$\frac{d^2\delta x}{d\tau^2}+\Omega^2\delta x=0 \tag{67}$$

$$\frac{d^2\delta z}{d\tau^2}-2\Omega^2\delta z=0 \tag{68}$$

$$\frac{d^2\delta\psi}{d\tau^2}-\frac{2}{\sigma_0}\Omega^4\delta x-\frac{5+2\sigma_0}{4}\Omega^2\delta z-2\Omega^2\delta\psi=0 \tag{69}$$

$$k_{11} = \sigma_0\sqrt{\frac{\sigma_0}{\nu}} - 3 - \frac{3}{64}(5+2\sigma_0)^2\sqrt{\sigma_0\nu} + \frac{1}{16}\frac{14\sigma_0+27}{\sigma_0}\nu + \mathcal{O}(\nu^{3/2})$$

$$k_{12} = \frac{3}{8}\sigma_0(5+2\sigma_0) - \frac{3}{32}(29+2\sigma_0)\sqrt{\frac{\nu}{\sigma_0}} - \frac{3}{1024}\frac{8\sigma_0^5+4\sigma_0^4+190\sigma_0^3+95\sigma_0^2+48\sigma_0-72}{\sigma_0^2}\nu + \mathcal{O}(\nu^{3/2})$$

$$k_{13} = \sigma_0 - \frac{1}{128}(5+2\sigma_0)^2\nu + \mathcal{O}(\nu^{3/2})$$

$$k_{21} = \frac{3}{8}\sigma_0(5+2\sigma_0) - \frac{3}{32}(29+2\sigma_0)\sqrt{\frac{\nu}{\sigma_0}} - \frac{3}{1024}\frac{8\sigma_0^5+4\sigma_0^4+190\sigma_0^3+95\sigma_0^2+48\sigma_0-72}{\sigma_0^2}\nu + \mathcal{O}(\nu^{3/2})$$

$$k_{22} = -2\sigma_0\sqrt{\frac{\sigma_0}{\nu}} + \frac{3}{64}(4\sigma_0^2+20\sigma_0+25)\sqrt{\nu\sigma_0} + \frac{1}{128}\frac{12\sigma_0^2-116\sigma_0-237}{\sigma_0}\nu + \mathcal{O}(\nu^{3/2})$$

$$k_{23} = \frac{1}{8}(5+2\sigma_0)\sqrt{\sigma_0\nu} - \frac{3}{32}\frac{(3-2\sigma_0)}{\sigma_0}\nu + \mathcal{O}(\nu^{3/2})$$

$$k_{31} = -2\frac{\sigma_0^2}{\nu} + \frac{1}{64}\sigma_0(4\sigma_0^2+20\sigma_0+25) - \frac{1}{128}(20\sigma_0^2+340\sigma_0-811)\sqrt{\frac{\nu}{\sigma_0}} + \\ + \frac{16\sigma_0^6+608\sigma_0^5+1400\sigma_0^4+440\sigma_0^3+6025\sigma_0^2-52800\sigma_0+68400}{16384\sigma_0^2}\nu + \mathcal{O}(\nu^{3/2})$$

$$k_{32} = -\frac{\sigma_0(5+2\sigma_0)}{4}\sqrt{\frac{\sigma_0}{\nu}} + \frac{1}{16}(26\sigma_0-71) - \frac{1}{256}\frac{(28\sigma_0^4-20\sigma_0^3+15\sigma_0^2-312\sigma_0+468)}{\sigma_0}\sqrt{\frac{\nu}{\sigma_0}} + \\ + \frac{4\sigma_0^5+432\sigma_0^4-1803\sigma_0^3+1935\sigma_0^2+324\sigma_0-486}{512\sigma_0^3}\nu + \mathcal{O}(\nu^{3/2})$$

$$k_{33} = -2\sigma_0\sqrt{\frac{\sigma_0}{\nu}} + 2 - \frac{1}{64}(4\sigma_0^2+20\sigma_0-39)\frac{\nu}{\sigma_0} + \mathcal{O}(\nu^{3/2})$$

Table 1: Values of the coefficients of the variational equations provided by the asymptotic analysis. These expressions have been calculated with Maple V

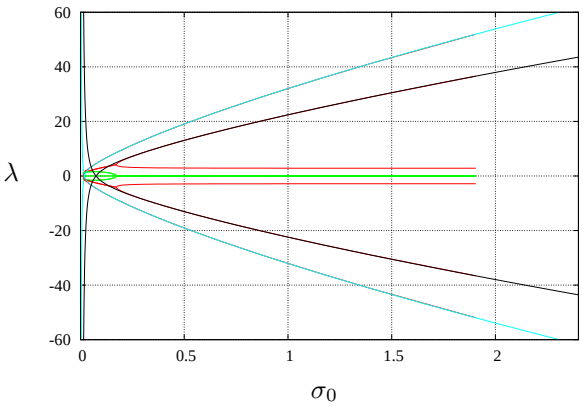

Figure 14: Eigenvalues of the matrix $\mathcal{M}$ for the main set of equilibrium positions. The numeric and the asymptotic solution for the most unstable eigenvalues are shown.

The most unstable eigenvalues of the matrix $\mathcal{M}$ are given by the following asymptotic expressions

$$\hat{\lambda}_1 = \pm\sqrt{2}\Omega\left(1 - \frac{2}{\Omega^4} - \frac{\sqrt{2}}{4}\frac{(2\sigma_0-5)\sigma_0}{\Omega^5} + \mathcal{O}(\Omega^{-6})\right)$$

$$\hat{\lambda}_2 = \pm\Omega\left(1 - \frac{11}{2\Omega^2} - \frac{417}{8\Omega^4} + \frac{(2\sigma_0-5)\sigma_0}{\Omega^5} + \mathcal{O}(\Omega^{-6})\right)$$

Figure 14 shows the agreement between the numeric and the asymptotic solution in the main set of equilibrium positions; only the most unstable eigenvalues have been plotted in the asymptotic solution. The agreement is excellent except for small values of σ where the pattern is more involved.

As consequence, it is possible to use the simplified equations (67-69) as the starting point of an additional analysis; this new analysis face the problem of finding some control law allowing the operation of the system in the neighborhood of one of these unstable equilibrium positions included in the *main set*. Such a control law should be carefully studied; the following results should only be considered as a first approximation to the control problem.

Control law

The solution of equations (67-69) is:

$$\delta x = A\sin(\Omega\tau + \phi_1) \tag{70}$$

$$\delta z = B\sinh(\sqrt{2}\Omega\tau + \phi_2) \tag{71}$$

$$\delta\psi = C\sinh(\sqrt{2}\Omega\tau + \phi_3) - \frac{2\Omega^2}{3\sigma_0}A\sin(\Omega\tau + \phi_1) + \frac{(5+2\sigma_0)\Omega}{8\sqrt{2}}B\tau\cosh(\sqrt{2}\Omega\tau + \phi_2) \tag{72}$$

It is clear that we have to consider a new time scale defined by $\Omega\tau \approx \mathcal{O}(1) \;\Rightarrow\; \tau \approx \mathcal{O}(1/\Omega)$. Moreover, the two sources of instability appear clearly in this solution: 1) the exponential growth of the variation δz and $\delta\psi$ and 2) the secular terms included in the right hand side of equation (72). Any strategy designed to control the system should face both.

Let us assume that a set of nominal conditions have been selected for the tethered system. The main parameter to be fixed is the average tether current, which depends on the ionospheric plasma density, the component of the electric field along the tether, the Jupiter magnetic field in the Amalthea orbit and the material characteristic of the tether. In such a case, σ has been fixed at a nominal value, $\sigma = \sigma_0$, and the tether is forced to work in the neighborhood of the equilibrium position (x_e, z_e, ψ_e) corresponding to this nominal value σ_0. For the sake of simplicity we will assume that this equilibrium position belongs to the *main set*. The following question arises: is it possible to introduce a reliable law for the tether current which permit to control the system?

Let us assume that the current is close to its nominal value. The parameter σ will be then

$$\sigma = \sigma_0 + u(\tau)$$

where $u(\tau)$ represent the deviation of the current, in non-dimensional terms, from its nominal value. Thus, success in this task implies that we are able to find an appropriate function $u(\tau)$ in such a way that the instability will be canceled. From a practical point of view, we can gain control on the system by means of a potentiometer —a variable resistance Z_T— placed at the cathodic end of the tether; thus, the variation of this resistance provides the desired variation of the current.

The variational equations take the form

$$\frac{d^2\delta x}{d\tau^2} - 2\frac{d\delta z}{d\tau} + k_{11}\delta x + k_{12}\delta z + k_{13}\delta\psi = -u(\tau)\sin\psi_e \tag{73}$$

$$\frac{d^2\delta z}{d\tau^2} + 2\frac{d\delta x}{d\tau} + k_{21}\delta x + k_{22}\delta z + k_{23}\delta\psi = +u(\tau)\cos\psi_e \tag{74}$$

$$\frac{d^2\delta\psi}{d\tau^2} + k_{31}\delta x + k_{32}\delta z + k_{33}\delta\psi = +k_{sb}u(t) \tag{75}$$

where k_{sb} is a parameter that depends on: 1) the mass distribution of the system, 2) the electrical and geometric characteristics of the tether 3) the ionospheric plasma density and 4) the motionless electric field generated by the motion of the tether into the Jupiter magnetic field. For a self-balanced electrodynamic tether it should be of order unity. In the derivation of these equations we assumed that the order of magnitude of the different variations $(\delta x, \delta z, \delta\psi)$ is the same as the order of magnitude of $u(\tau)$.

Note that by neglecting the attitude problem (eq. (75)) and taking the asymptotic version of the equations, we find

$$\frac{d^2\delta x}{d\tau^2} + \Omega^2\delta x = 0 \tag{76}$$

$$\frac{d^2\delta z}{d\tau^2} - 2\Omega^2\delta z = u(\tau) \tag{77}$$

With this simplified model, the value of $u(\tau)$ could be selected, for example, as

$$u(\tau) = -3\Omega^2\delta z$$

in order to obtain stability for the system, because the variable δz becomes stable. Indeed, this choice for the control function $u(\tau)$ provides that the unstable equation (77) becomes

$$\frac{d^2\delta z}{d\tau^2} + \Omega^2 \delta z = 0$$

and the time evolution of δz would be oscillatory, as in the case of the variation δx.

This simple control law shows that the response time should be of order unity, or smaller, in the new time scale $\Omega\tau \approx \mathcal{O}(1)$. Obviously this result can be improved and we hope to do so, considering in more detail the necessary safety factors involved in any mission similar to the one proposed in these pages.

However, the detailed analysis of the full control problem including the attitude of the system is more involved. It requires the determination of the factor k_{sb} in terms of the characteristics of the tether; fortunately the theory needed to do that is fully developed. It is not the same with the external field in the neighborhoods of Jupiter; at present, however, these models are being improved. An option that must be assessed is the possibility of using a part of the electrical energy generated in the S/C in order to help to the stabilization of the system. All these tasks related with the control problem will be undertaken in future papers.

Conclusions

In this paper we propose a system that allows one to obtain electrical energy in a continuous way by deorbiting one of the Jupiter inner moonlets (Metis, Adrastea, Amalthea, Thebe) with the help of a self-balanced electrodynamic tether. We take Amalthea as example but further analysis should be carried out to elucidate the best candidate. Obviously, and due to the huge mass of the moonlet, it is possible to obtain a significant amount of energy with quite negligible decay of the moonlet.

Two different analyses have been carried out. In the first one, the attitude problem is neglected; we obtain equilibrium positions that are unstable in the neighborhoods of the moonlet. In the second one, the attitude of the tethered system is taken into account. We again obtain equilibrium positions similar, from a qualitative point of view, to the ones obtained in the previous analysis. Moreover, the quantitative differences are not significant. Using asymptotic techniques we obtain asymptotic solutions for the equilibrium positions.

We carried out a linear stability analysis to show the unstable character of these equilibrium positions which leads to a control problem that has been partially formulated. Such a control problem represent the natural continuation of this paper and will be faced in further works. The asymptotic analysis performed for the stability properties of the system permits one to describe clearly the significant regions and time scales involved in the analysis. However, in this sense we should note that the self-balanced electrodynamic tether concept has been selected. The inclination of the moonlet orbits is very small and therefore, the instabilities associated with a non-vanishing inclination will be very small also. As a consequence, the tether current can be used to control the S/C in the nominal —unstable— equilibrium positions more easily.

Acknowledgements

The work of J. Peláez was carried out in the framework of the research project entitled **Dynamics of satellite orbit descent/raise using electrodynamic tethers** (ESP2004-04376) supported by the DGI of the Spanish Ministry of Education and Science.

References

[1] **J. R. Sanmartín, M. Martínez-Sánchez & E. Ahedo**, "Bare Wire Anodes for Electrodynamic Tether", *Journal of Propulsion and Power*, 9(0):352–320, 1993.

[2] **R. I. Samanta Roy, D. E. Hastings and E. Ahedo**, "Systems analysis of electrodynamic tethers," *Journal of Spacecraft and Rockets*, Vol. 29, 1992, pp. 415–424.

[3] **G. Vannaroni, M. Dobrowolny and F. De Venuto**, "Deorbiting of LEO Satellites with Electrodynamic Tethers", *Proceedings Aerospace Sciences Meeting and Exhibit*, January, 2000.

[4] **J. Corsi & L. Iess**, "Stability and Control of Electrodynamic Tethers for De-orbiting Applications," *Acta Astronautica*, Vol. 48, No. 5-12, 2001, pp. 491–501.

[5] **L. Iess, C. Bruno, C. Ulivieri, et al.**, "Satellite de-orbiting by means of electrodynamic tethers - Part I: General concepts and requirements," *Acta Astronautica* , Vol. 50(7), April 2002, pp.. 399–406

[6] **L. Iess, C. Bruno, C. Ulivieri, et al.**, "Satellite de-orbiting by means of electrodynamic tethers - Part II: System configuration and performance," *Acta Astronautica* , Vol. 50(7), April 2002, pp.. 407–416

[7] **J. Peláez & M. Sanjurjo**, "Power generation using self-balanced electrodynamic tethers in debris mitigation scenarios" (Paper AAS07-196) of *The 2007 AAS/AIAA Space Flight Mechanics Meeting Sedona, Arizona, January 28 - February 1, 2007.*

[8] **E. Ahedo and J. R. Sanmartin**, "Analysis of bare-tethers systems for deorbiting Low-Earth-Orbit satellites," *Journal of Spacecraft and Rockets*, Vol. 39, No. 2, March-April, 2002, pp. 198–205.

[9] **J. Peláez**, "Self balanced electrodynamic tethers," *Paper AIAA 2004-5309, The 2004 AAS/AIAA Astrodynamics Specialist Conference and Exhibit*, Providence, Rhode Island, USA, 16-19 August 2004.

[10] **J. Peláez, M. Sanjurjo & J. Fontdecaba**, "Satellite deorbiting using a self balanced electrodynamic tether," *Paper IAC-04-A.5.08, The 55th International Astronautical Congress*, Vancouver, Canada, October 2004.

[11] **J. Peláez & M. Sanjurjo**, "Generator regime of self balanced electrodynamic bare tethers" *Advances in the Astronautical Sciences*, Vol.120 (PART II), pp. 1651-1670, 2005.

[12] **J. Peláez & M. Sanjurjo**, "Generator regime of self balanced electrodynamic bare tethers" *Journal of Spacecraft and Rockets*, Vol. 43, # 6, November-December 2006, pp. 1359-1369.